Title: Arctic and Antarctic sea ice state in the Community Earth System Model Version 2

Authors: Alice K. DuVivier[1], Marika M. Holland[1], Jennifer E. Kay[2], Simone Tilmes[1], Andrew Gettelman[1], David A. Bailey[1]

[1] National Center for Atmospheric Research, Boulder, CO

[2] Department of Atmospheric and Oceanic Sciences and Cooperative Institute for Research in Environmental Sciences, University of Colorado at Boulder, Boulder, CO

Date of submission:

Dec. 2019, JGR-Oceans

Corresponding author:

Alice K. DuVivier, CGD, P.O. Box 3000, Boulder, CO 80307

Email: duvivier@ucar.edu

Key Points:

1. Simulated sea ice matches Arctic and Antarctic observed mean extent and volume, and Arctic observed historic trends.
2. The Arctic sea ice state differs significantly due to cloud-aerosol radiative impacts resulting from the inclusion of prognostic aerosols.
3. Phenology of preindustrial Arctic liquid clouds drives differences in the ice-albedo feedback and the amount of summer ice loss.

Abstract

Arctic and Antarctic sea ice has undergone significant and rapid change with the changing climate. Here, we present preindustrial and historical results from the newly released Community Earth System Model Version 2 (CESM2) to assess the Arctic and Antarctic sea ice. Two configurations of the CESM2 are available that differ only in their atmospheric top of the atmosphere height and the inclusion of comprehensive atmospheric chemistry, including prognostic aerosols. The CESM2 configuration with comprehensive atmospheric chemistry has significantly thicker Arctic sea ice year-round and better captures observed decreasing trends in sea ice extent and volume. In the Antarctic, the two configurations have similar ice extent as observations, but the ice extent decreases during the historical period contrary to observations. We find that differences in the Arctic sea ice are the result of differences in liquid clouds. Over the Arctic, the CESM2 configuration without prognostic aerosol formation has fewer aerosols to form cloud condensation nuclei and thinner liquid clouds. As a result, the sea ice receives much more shortwave radiation early in the melt season, driving a stronger ice-albedo feedback and leading to additional sea ice loss and significantly thinner ice year-round. The aerosols necessary for the Arctic liquid cloud formation are produced from different precursor emissions and transported to the Arctic. In contrast, in the relatively pristine Antarctic there are insignificant differences between CESM2 configurations in aerosol concentration, liquid cloud cover, and surface radiative fluxes, so the sea ice thickness and concentration in the Antarctic is similar between CESM2 configurations.

1. Introduction

Recent rapid and substantial changes in the polar regions include warming oceans and transformation of the Arctic and Antarctic sea ice cover (Parkinson, 2014; Meredith & Sommerkorn, 2019). The Arctic sea ice cover has become thinner (Lindsay & Schweiger, 2015; Kwok, 2018) and less extensive (Stroeve & Notz, 2018). Satellite observations since 1979 show that decreases in Arctic sea ice extent occur in all months and that the twelve lowest September sea ice extents were recorded in the past twelve years (Richter-Menge et al., 2019). In the Antarctic, after decades of increasing Antarctic sea ice extent, there was a dramatic decrease in ice extent in 2016 (Stuecker et al., 2017; Turner et al., 2017; Meehl et al., 2019).

In the physical earth system, changes to sea ice have the capacity to impact local boundary layer clouds, temperature, and humidity, which can feedback on sea ice evolution (Kay & Gettelman, 2009; Boisvert & Stroeve, 2015; Morrison et al., 2018; Huang et al., 2019) and the large-scale atmospheric circulation (e.g., Alexander, 2004; Barnes & Screen, 2015; Deser et al., 2016). Additionally, changing sea ice impacts the ecosystem and human infrastructure (Hunter et al., 2010; Kovacs et al., 2011; Jenouvrier et al., 2014; Moon et al., 2019). In order to assess possible future sea ice changes and their impacts with confidence, we must evaluate our historical climate model representations of the sea ice state.

The Community Earth System Model (CESM) and its various iterations have been used widely to understand the changing Arctic and Antarctic. Recent work has highlighted the

63 impact of internal climate variability on the possible range of Arctic and Antarctic sea ice
64 conditions (Mahlstein et al., 2013; Swart et al., 2015; Jahn et al., 2016). Previous versions
65 of the CESM have performed well in capturing the Arctic mean sea ice state, trends, and
66 variability (e.g. Holland et al., 2006; Kay et al., 2011a; Jahn et al., 2012; Barnhart et al.,
67 2015; Jahn et al., 2016; DeRepentigny et al., 2016; Labe et al., 2018). In the Antarctic,
68 however, previous versions of CESM have too extensive sea ice cover and are unable to
69 replicate observed trends in sea ice extent, even when accounting for potential effects of
70 internal variability (Landrum et al., 2012; Mahlstein et al., 2013). Additionally, extensive
71 work has been done to assess the impact of clouds on Arctic climate change and place
72 cloud feedbacks in the context of other processes and feedbacks (e.g. Kay et al., 2012;
73 Pithan & Mauritsen, 2014; Goosse et al., 2018). Detailed process-level assessment is
74 essential to understand the contribution of clouds to simulated Arctic change in models
75 and assess their realism. For example within CESM, some versions of the atmospheric
76 model with CESM have credibly represented cloud-sea ice feedbacks for the right
77 reasons (e.g. CAM5, Morrison et al., 2019), while others have not (e.g. CAM4, Kay et
78 al., 2011b).
79
80 CESM version 2 (CESM2) has been publicly released and data from two configurations –
81 CESM2(CAM6) and CESM2(WACCM6) (hereafter called CAM6 and WACCM6) – are
82 freely available from the Coupled Model Intercomparison Project Phase 6 (CMIP6)
83 archive. The purpose of this manuscript is 1) to document the Arctic and Antarctic sea ice
84 in the two CESM2 configurations over the historical and preindustrial (PI) periods, and 2)
85 investigate the source of differences in the mean sea ice state. Section 2 describes the two

86 CESM2 configurations used in this analysis and highlights the differences in simulations.
87 We examine the PI and historical mean sea ice state in the Arctic and Antarctic in section
88 3. In section 4, we investigate the differences in PI sea ice surface energy budget, mass
89 budget, and clouds focusing primarily on the Arctic. Finally, section 6 comprises a
90 discussion and conclusions.
91
92 **2. Data and Methods**
93 *2.1 The Community Earth System Model Version 2 (CESM2)*
94 The CESM2 is a freely available, community-developed fully coupled earth system
95 model. The model components are atmosphere, ocean, land, sea ice, and land ice models
96 that exchange information through a flux coupler. The major new features and
97 capabilities of CESM2 have been documented in Danabasoglu et al. (2019) and
98 additional details about the CESM2 experiments contributed to CMIP6 can be found
99 there as well. In this manuscript we will discuss in detail only the components relevant to
100 the analysis presented.
101
102 Two versions of CESM2 were contributed to the CMIP6 effort and differ only in their
103 atmospheric configuration. The CAM6 experiments use the Community Atmosphere
104 Model version 6 (CAM6; Neale et al., 2019) while the WACCM6 experiments use the
105 Whole Atmosphere Community Climate Model version 6 (WACCM6; Gettelman et al.,
106 2019). Both CESM2 configurations use nominal 1° (1.25° longitude x 0.9° latitude)
107 horizontal resolution, the same finite volume dynamical core, and identical
108 parameterization tuning. A major difference between the atmospheric models is that

CAM6 has 32 vertical levels with the model top in the stratosphere at 3.6 hPa (~40 km) while WACCM6 has 70 vertical levels with a model top in the lower thermosphere at $6x10^{-6}$ hPa (~140 km). The vertical level spacing is identical between CAM6 and WACCM6 from the surface to 87 hPa. Another major difference is that WACCM6 has comprehensive chemistry with 228 prognostic chemical species and prognostic aerosols. Those include the formation of secondary organic aerosols (SOA) from precursor emissions using the volatility basic set (VBS) approach (Tilmes et al., 2019) and interactive stratospheric aerosols (Mills et al., 2017). On the other hand, CAM6 has limited chemistry and prescribes tropospheric and stratospheric oxidants that feed the aerosol model. As detailed in Danabasoglu et al. (2019), these oxidants in CAM6 were obtained from WACCM6 simulations in order to use consistent forcings in both CAM6 and WACCM6 simulations.

The sea ice and ocean models are identical in the CAM6 and WACCM6 configurations, and they share a horizontal grid. The horizontal resolution is a uniform 1.125° in the zonal direction. The resolution varies in the meridional direction: in the Arctic, the minimum resolution is approximately 0.38° in the northwestern Atlantic Ocean while in the northwestern Pacific Ocean the maximum resolution is about 0.64°, and in the Antarctic the resolution is constant at 0.53°. To represent sea ice, CESM2 uses the CICE model version 5.1.2 (Hunke et al., 2015). Both configurations of CESM2 have identical sea ice physics and parameters, and both use the new mushy-layer thermodynamics (Turner & Hunke, 2015; Bailey et al., 2019) as well as updates to the melt pond parameterization (Hunke et al., 2013). In these experiments, CICE uses eight vertical ice

132 layers and three vertical snow layers in order to better represent the vertical salinity and
133 temperature profiles. CESM2 uses the Parallel Ocean Program version 2 (Smith et al.,
134 2010) as described in (Danabasoglu et al., 2012) with updates as discussed in
135 Danabasoglu et al. (2019). Both the CESM2 configurations use identical ocean physics.
136
137 The CAM6 and WACCM6 PI simulations were integrated 1200 and 500 years,
138 respectively. Over this period the global mean top of atmosphere heat imbalances were
139 small at +0.05 and +0.06 W m^{-2}, respectively, and this gain is reflected only in the ocean
140 simulation (Danabasoglu et al., 2019). For the historical (1850-2014) period there are 11
141 CAM6 and three WACCM6 ensemble members. The historical CAM6 and WACCM6
142 experiments were branched from random years in the respective PI experiments. Both the
143 CAM6 PI and historical experiments used realistic chemical and aerosol constituents
144 forcing derived from the WACCM PI control (for PI) and an average of the three
145 historical WACCM6 experiments (for historical).
146
147 When analyzing the historical experiments, we focus on the years 1979 to 2014 (36
148 years) in order to compare with the satellite observational record. For the PI analysis we
149 analyze the years 100-500 in each experiment. We omit the first 100 years of each
150 simulation as the model was spinning up, and we analyze only overlapping years to
151 minimize the likelihood that differences in the CAM6 and WACCM6 experiments are a
152 result of the model drift from the much longer CAM6 PI. We use the variables output for
153 the Sea Ice Model Intercomparison Project (SIMIP; Notz et al., 2016). Welch's t-test,
154 which does not assume equal variance for the samples, was used to determine

155 significance of differences in mean values; an F-test was used to determine significance
156 between differences in variance.

157

158 *2.2 Observational datasets for comparison*

159 Over the historical period (1979-2014), we compare the hemispheric average annual sea
160 ice extent timeseries and annual cycle against the hemispheric sea ice index (Fetterer et
161 al., 2017). The spatial locations of the observed ice edge - defined as 15% concentration -
162 are derived from the SSMR and SSM/I satellite data (Comiso, 2000). Unlike for sea ice
163 extent, year-round, long-term gridded sea ice thickness data over the Arctic and Antarctic
164 Oceans are not available. Instead, over the historical (1979-2014) period we compare
165 both Arctic and Antarctic sea ice volume with the Global Ice-Ocean Modeling and
166 Assimilation System (GIOMAS; Zhang & Rothrock, 2003). In the Arctic, the Pan-Arctic
167 Ice-Ocean Modeling and Assimilation System (PIOMAS; Schweiger et al., 2011), and
168 five years of gridded ICESat satellite sea ice thickness data for the spring (FM; 2003-
169 2007) and autumn (ON; 2004-2008) (Kwok et al., 2009) are also available for
170 comparison. Finally, a new, longer-term Arctic sea ice thickness and volume product
171 based on satellite-derived ice age is also used for comparison (Liu et al., 2019).

172

173 **3. Arctic Sea Ice Mean State in the Preindustrial and Historical Periods**

174 *3.1 Sea ice areal coverage*

175 Evaluating the area of the oceans covered by sea ice is important for understanding the
176 planetary energy budget. In the Arctic, for both the PI and historical experiments, the

177 CAM6 sea ice extent is smaller than the WACCM6 extent (Fig.1a,1b; Table 1). The
178 hemispheric sea ice extent for overlapping PI years 100-500 is significantly larger for the
179 WACCM6 configuration compared to the CAM6 configuration. The ensemble mean
180 extent for WACCM6 is significantly higher than the CAM6 ensemble mean for 23 of the
181 36 years in the historical period. The observed Arctic sea ice extent falls within the
182 WACCM6 ensemble spread, while the CAM6 ensemble spread tends to be lower than the
183 observed sea ice extent. Both configurations lose sea ice over the PI and historical
184 periods, but the historical rate of loss is two orders of magnitude larger than in the PI
185 period due to transient greenhouse gas forcing (Table 2). The rate of historical loss from
186 both CESM experiments compares well with observations.
187
188 We examine the Arctic sea ice extent seasonal cycle to identify any systematic seasonal
189 differences between CAM6 and WACCM6. In both the PI and historical periods, the
190 WACCM6 hemispheric extent is significantly higher than CAM6 for all months, though
191 the difference is smallest in winter months (Fig.2a). In the historical period the maximum
192 modeled ice extent occurs in March. The winter ice extent is lower than observed, mainly
193 due to less ice coverage in the Pacific, including the Bering Sea and Sea of Okhotsk
194 (Fig.3a). In both the PI and historical periods, the CAM6 experiments have less extensive
195 winter ice then WACCM6, which is due to less ice coverage on both the Atlantic and
196 Pacific margins of the sea ice pack with the largest differences occurring in the Atlantic
197 sector (Fig.3c; Supp. Fig.1). The rate of spring ice loss for CAM6 is similar to observed
198 until July, while the WACCM6 loss is slower than observed (Fig.2a). Ultimately, both
199 CESM configurations reach the minimum ice extent in September, though the WACCM6

ice extent is much closer to observed than CAM6. The CAM6 mean September minimum extent is significantly lower than WACCM6 in both the PI and historical periods by $1x10^6$ km^2 and $2x10^6$ km^2 respectively (Fig.2a). The WACCM6 ensemble mean summer extent is similar to observations in the hemispheric average and spatial coverage of sea ice (Fig.2a, 3b). In contrast, the historical CAM6 summer sea ice extent is too low over much of the Arctic Basin with the largest difference in the East Siberian Sea (Fig.3d). A similar difference in ice concentration focused in the East Siberian Sea exists in the PI period between CAM6 and WACCM6 (Supp. Fig.1).

We examine the sea ice extent variability, as quantified by the standard deviation. There is greater variability throughout the year in the historical period compared to the PI (Fig.2b). In both time periods the summer variability is higher than the winter variability because the winter variability is constrained primarily by the land boundaries and ocean heat content (Bitz et al., 2005). The year-round increase in variability in the historical period is likely due to thinner sea ice (Goosse et al., 2009; Holland et al., 2008), and the increase is particularly large in summer months. The WACCM6 historical summer variability is more similar to observed variability, and it is significantly lower than the CAM6 variability likely due to differences in the ice thickness.

3.2 Sea ice thickness

Understanding sea ice thickness, in addition to concentration and extent, is particularly important because the ice thickness is an important factor in sea ice predictability. The PI annual mean Arctic ice volume is significantly larger ($4.7x10^3$ km^3) for the WACCM6

than CAM6 (Fig.1c; Table 1), and over the historical period the ensemble mean sea ice volume is significantly different every year with differences as large as $8x10^3$ km^3 (Fig.1d). The reconstructed mean sea ice volume from PIOMAS and GIOMAS is more similar to the WACCM6 ensembles and mean, particularly later in the historical period (Fig.1d). The historical rate of ice volume loss is higher in WACCM6 than CAM6, and the CAM6 rate compares better with reconstructed loss rates (Table 2). In every month, in both the PI and historical periods, the CAM6 sea ice volume is significantly lower than the WACCM6 sea ice volume (Fig.2c). While the WACCM6 monthly mean ice volume is more similar to the PIOMAS and GIOMAS products, the timing of the WACCM6 ice volume loss is delayed by a month compared to the reconstructed volume and remains a bit higher during the annual September minimum. Despite the differences in mean ice volume, the variability is not significantly different between the CAM6 and WACCM6 configurations during the PI (Fig.2d). However, the variability is significantly different in the historical period when CAM6 variability is more similar to the reconstructed variability.

When we examine just the Central Arctic over the historical period, we find that the mean WACCM6 ice volume compares well against newly available satellite derived data (Supp. Fig.2). In this region, the WACCM6 ensemble mean has a higher fraction of thicker ice than CAM6 in both spring and autumn (Fig.4). While the ICESat observations and WACCM6 peaks in ice fraction of similar ice thicknesses, the ICESat observations have higher fractions of very thick ice in both seasons (Fig.4). While the modeled ice is thinner than observed across the entire Central Arctic in both seasons, the largest

differences with ICESat occur along the Canadian Arctic Archipelago and are co-located with the thickest sea ice (Fig.5). When we examine a longer historical period and the PI records, neither of which have observations against which we can compare, we find that the ice thickness distributions between the CAM6 and WACCM6 remain distinct in the Arctic. In each time period, WACCM6 has a higher fraction of thicker ice in both winter and summer (Supp. Fig.3), and the spatial thickness differences occur in the East Siberian Sea region (Supp. Fig.4; Supp. Fig.5).

4. Exploring Differences in Preindustrial Arctic Sea Ice

Given the small differences in CESM2 configurations, the differences in the mean Arctic sea ice extent and volume are surprising. We examine the forcing and processes that govern ice growth and melt in order to better understand these mean state differences. Many of the differences between CAM6 and WACCM6 exist in both the historical and PI periods, but the following analysis corresponds to PI years 100-500 for both CAM6 and WACCM6 because there are many years for analysis without the possible additional influence of transient atmospheric forcing. We focus on the region north of 70°N since it has the largest differences in ice thickness and extent (Supp. Fig.1; Supp. Fig.5).

4.1 Northward Heat Transport

Northward heat transport (NHT, watts) into the polar regions results from a combination of atmospheric northward heat transport, oceanic northward heat transport, and sea ice export and the resulting latent heat loss from the ice melt. We calculate NHT following

Kay et al. (2012) to identify whether differences in heat flux convergence between CESM2 configurations could account for the differences in Arctic sea ice mean state. The NHT at a given latitude can be divided by the Earth's surface area north of that latitude to obtain a NHT forcing (W m^{-2}) that can be directly compared to other forcing (e.g. radiative). We find that in both the CAM6 and WACCM6 configurations the atmospheric component of the NHT dominates the total NHT, which peaks at about 6 Petawatts, while the sea ice component is the smallest (Supp. Fig.6a). The net differences between the configurations are small (less than 2% the total NHT) and primarily due to atmospheric NHT (Supp. Fig.6b). When we examine the NHT differences as a forcing we find that over the Arctic WACCM6 has 2-4 W m^{-2} higher NHT than CAM6 (Fig.6a). This suggests that, given NHT alone, WACCM6 might be expected to have less extensive and thinner ice, which is the opposite to our results and implies another cause for the differences in CESM2 configurations. Additionally, there are not significant differences in global or Northern Hemisphere surface temperature climate between CESM2 configurations during the overlapping simulation years (Table 1). We also find statistically insignificant differences in mean sea level pressure and surface winds in the Arctic (not shown), which suggests atmospheric circulation differences that could impact the sea ice dynamics and drive differences in thickness are not responsible.

4.2 Mass and Energy Budgets

We examine the annual cycle of the sea ice mass budget to determine causes driving the differences in ice growth and melt. There is net growth from September to May, mainly due to congelation sea ice growth at the bottom of the ice (Supp. Fig.6c). During the

291 growth season, CAM6 has more ice growth, due primarily to congelation ice, than
292 WACCM6 (Fig.6b). The increased ice growth for the CAM6 configuration is likely due
293 to the thinner ice, which is less insulating, allowing for increased heat conduction through
294 the sea ice (Maykut, 1982). Both configurations have net ice mass loss from May through
295 August that is dominated by bottom melt (Fig.6b; Supp. Fig.6c). Increased summertime
296 bottom melt in CAM6 dominates the net mass budget differences, though in June and
297 July CAM6 has significantly more loss from top melt as well.

298

299 To investigate differences in the sea ice mass budget, we also examine differences in the
300 annual surface energy budget north of 70°N. We examine both the surface energy budget
301 for sea ice alone as well as the combined ice and ocean surfaces. The ice surface loses
302 heat from September to May (Fig.6c), which corresponds to the period of net ice mass
303 gain (Fig.6b). In the autumn (October-November) the CAM6 ice surface loses ~7 Wm^{-2}
304 more than in WACCM6 (Fig.6c), which corresponds to the increase in congelation
305 growth at this time (Fig.6b). From June to August both the CAM6 ice surface and total
306 ice plus ocean surface gain a maximum of ~4Wm^{-2} more than the WACCM6 surface
307 (Fig.6c). The largest driver of the difference in the surface energy budgets are the
308 downward shortwave and longwave radiative components (Fig.6c). In particular, CAM6
309 has over 10 Wm^{-2} more incoming shortwave radiation, which is compensated some by ~6
310 Wm^{-2} less incoming longwave radiation, to both surfaces compared to WACCM6. The
311 incoming radiative differences are largest in May, but they persist through the melt
312 season. As expected with near-freezing surface temperatures throughout the melt season,
313 the outgoing longwave radiation is similar between the configurations during the melt

314 season. The outgoing shortwave radiation is also a bit higher in the CAM6 experiment,
315 which is likely due to the more incoming shortwave, not an increase in albedo.
316
317 Changes in surface albedo over sea ice are due to changes in ice surface conditions (the
318 loss of snow cover coupled with the increase in melt pond coverage), while the
319 differences in the total surface albedo are due to the combination of ice surface changes
320 and changes in ice fraction. CAM6 has a lower ice albedo and total surface albedo than
321 WACCM6, and the differences from WACCM6 are largest in August (Fig.7a). The
322 divergence between the ice albedo and surface albedo differences indicates that changes
323 in ice fraction between CAM6 and WACCM6 become increasingly important later in the
324 melt season. The phenology of the melt season is important for driving these changes.
325
326 Indeed, the changes to the surface albedo and the resulting albedo feedback are likely
327 responsible for the mismatch in timing of maximum shortwave radiation differences
328 (May) and the maximum melt differences (July). In May and June, the sea ice is covered
329 by snow and the ice fraction is relatively similar between CAM6 and WACCM6 (Fig.7b).
330 Additional incoming solar energy in CAM6 results primarily in increased surface snow
331 melt and not top melt of the ice itself (Fig.6b; Fig.7c). As a result of earlier surface snow
332 melt, the ice albedo in CAM6 decreases due to both the combination of bare ice and melt
333 pond coverage. The change in ice surface albedo results in increased solar absorption,
334 increased ice top melt, and a sharper decrease in sea ice fraction. As a result of the
335 decrease in ice coverage, the ocean absorbs solar radiation. This ocean energy gain drives
336 large differences in bottom melt by July, melting more ice.

The differences in NHT indicate that the CAM6 experiments have less heat flux convergence from lower latitudes into the Arctic as compared to WACCM6. This cannot explain the thinner ice present in the CAM6 simulations. Instead, the differences in mean ice state between CAM6 and WACCM6 are related to local differences in radiation. The difference in radiation triggers the ice-albedo feedback earlier in the CAM6, and this feedback amplifies the differences in ice state later in the melt season when the radiative differences are smaller. It is important to understand how the CESM2 configurations differ that leads to the large differences in radiative forcing.

4.3 *Clouds*

We examine differences in the Arctic shortwave feedbacks north of 70°N to investigate their impact on the difference in mean sea ice state in the CESM2 configurations. Of particular interest are 1) the positive shortwave surface feedback – melting ice and snow lower surface albedo, increasing surface shortwave absorption; and 2) shortwave cloud feedbacks – for example, the negative shortwave cloud feedback that results from increases in liquid water resulting in higher cloud albedo and decreasing surface shortwave absorption (Goosse et al., 2018). We evaluate these feedbacks using the approximate partial radiative perturbation (APRP) method (Taylor et al., 2007). During the summer melt season, we see that the combination of the surface albedo and cloud shortwave feedbacks lead to greater shortwave forcing in CAM6 than WACCM6, and that the magnitude of the cloud term differences is larger than the surface term (Fig.8a). For the positive surface albedo feedback, the positive difference indicates that CAM6 has

a larger surface albedo feedback, which is expected given the differences in surface albedo discussed previously. For a negative cloud feedback, the positive difference indicates that CAM6 has a smaller cloud feedback than WACCM6.

We examine differences in the Arctic cloud properties north of 70°N to identify how the clouds differ throughout the year in CAM6 and WACCM6. The liquid water path (LWP) is defined as the sum of the total liquid water in the atmospheric column, and similarly the ice water path (IWP) is defined as the sum of the total ice water in the atmospheric column. Compared to WACCM6, CAM6 has both lower LWP and IWP through the summer months (Fig.8b). In May, CAM6 has ~22% lower LWP than WACCM6, and in June CAM6 has ~25% less IWP. Throughout the year both configurations have cloud fractions above 80% and the difference in cloud fraction between the two configurations is never greater than 4% (Fig.8b). Maps of cloud property differences show large and significant differences in LWP all summer that are co-located with the sea ice (Fig.9). In contrast, the absolute differences in IWP and cloud fraction are more hemispheric, though maps of percent differences show that the largest percent differences occur over the Arctic sea ice (Fig.9; Supp. Fig.7).

As described in Section 2, the CESM2 configurations that use CAM6 and WACCM6 have identical sea ice parameters and atmospheric cloud parameters. One important way they differ, however, is with the inclusion of comprehensive chemistry and prognostic aerosols including an improved formation of SOA within the WACCM6 (see Tilmes et al., 2019). During spring there are fewer accumulation mode SOA, primary organic

matter, black carbon, and sulfate aerosols over sea ice in CAM6 as compared to WACCM6 (Fig.10). These differences in aerosol are similar in summer for all aerosols except the SOA. In addition to fewer aerosols, there are also fewer liquid cloud condensation nuclei (CCN) and cloud droplets in CAM6 as well (not shown). Thus, in WACCM6 the improved aerosol formation in source regions outside the Arctic leads to an increase in the aerosols in the accumulation mode and therefore the amount of CCN reaching the Arctic. In the WACCM6 configuration, more Arctic CCN tend to result in more and smaller cloud drops. As a result, there is less precipitation, a longer lifetime for cloud drops, and higher LWP and cloud fractions, which results in reduced shortwave flux to the surface.

5. Antarctic Sea Ice Mean State in the Preindustrial and Historical Periods

5.1 Sea ice areal coverage

In the Antarctic, we find that CAM6 and WACCM6 do not have statistically different mean extent for overlapping PI years 100-500 (Table 1), and the sea ice extents overlap (Fig.11a). The WACCM6 sea ice extent is significantly greater when we compare it with the full CAM6 PI (years 100-1200), but this difference can be attributed to the PI drift over the additional CAM6 700 years (Table 2). The two CESM configurations maintain similar sea ice extent over the historical period when there are significant differences in the annual mean ice extent over only six years of the historical period (Fig.11b). All ensemble members from both configurations and the resulting ensemble mean lose sea ice over the historical period, while the observed trend is positive (Table 2). The historical loss rate is two orders of magnitude larger than the PI rate, indicating that

differences in forcing rather than model drift are likely to drive the historical trends. The discrepancy in the sign of modeled and observed trends in Antarctic sea ice have been previously documented for climate models (e.g. Hobbs et al., 2015; Landrum et al., 2012; Mahlstein et al., 2013). The recent observations of dramatic loss in Antarctic sea ice (Stuecker et al., 2017; Meehl et al., 2019; Wang et al., 2019) occurred after the CMIP6 historical forcing period and are still being investigated.

The annual cycle of Antarctic sea ice extent in the PI and historical periods is similar for both the CAM6 and WACCM6 experiments (Fig.12a). While the timing and magnitude of the historical minimum February sea ice extent agree well with NSIDC observations the maximum extent occurs in October and is ~$2x10^6 km^2$ smaller than the observed maximum in September. There is no significant difference in ice extent variability in the PI, though there is in the historical. Spatially, the WACCM6 maximum ice concentration is too low in the Indian sector of the Antarctic basin (Fig.13b). While the ice concentration differences between CAM6 and WACCM6 are heterogenous and mostly insignificant, in winter months CAM6 has lower extent in the Atlantic and Indian sectors compared with WACCM6 (Fig.13). In the PI period, however, CAM6 has slightly higher ice concentration in the wintertime Indian and Pacific sectors (Supp. Fig.8).

5.2 Sea ice thickness

The Antarctic the PI hemispheric mean ice volume is fairly similar, though the annual mean volume for WACCM6 over years 100-500 is higher than CAM6 (Table 1; Fig.11c). During the historical period there are only four years in which the ensemble mean volume is significantly different (Fig.11d), and both the CESM2 configurations have a negative

ice volume trend while observationally reconstructed trends are positive (Table 2). Neither configuration captures the magnitude or the timing of the minimum or maximum volume, and the volume is most different between configurations during wintertime (Fig.12c). Histograms indicate that in both the historical and PI the distribution of winter thickness fractions is similar in CAM6 and WACCM6, but there are slight differences in summer historical distributions (Supp. Fig.3). Spatially, the differences in historical thickness are primarily located at the ice edge or in the Weddell Sea, and similarly insignificant and heterogeneous patterns are seen in the PI (Supp. Fig.9). Indeed, an examination of the mass and energy budgets (Supp. Fig.10) shows that there are not significant differences in the net budgets in the Antarctic, which is consistent with the very similar mean state.

6 Discussion and Conclusions

We present the Arctic and Antarctic sea ice mean state from available PI and historical experiments from two configurations of the CESM2 submitted to CMIP6. In the Arctic, there is a significant difference in sea ice extent and thickness in both the PI and historical periods between the CAM6 and WACCM6 configurations, and WACCM6 has thicker and more extensive ice. In the historical period, both CESM2 configurations well capture the decreasing trends in ice extent and ice volume observed over the historical period as well as timing of the seasonal cycle in ice extent and volume. In the winter, both configurations underestimate the maximum ice extent, but in summer the WACCM6 minimum sea ice extent is very similar to observed while the CAM6 sea ice extent is significantly lower. In both the PI and historical periods, the WACCM6 sea ice is

452 significantly thicker over the Arctic Basin throughout the year as compared to CAM6.
453 While the WACCM6 ice thickness is closer to observations, the model still fails to
454 capture the very thick ice observed along the Canadian Archipelago. There are significant
455 differences in the extent and volume variability between configurations as a result of the
456 sea ice thicknesses differences between the configurations.

457

458 In the Antarctic, the CAM6 and WACCM6 configurations are very similar in ice extent
459 and thickness throughout the year. While both CESM2 configurations have sea ice
460 extents similar to those observed, all ensembles have a decreasing trend in ice extent,
461 contrary to observations. Additionally, both CESM2 configurations capture the Antarctic
462 minimum extent but tend to underestimate the maximum extent and it occurs one month
463 after the observed maximum. In contrast to the Arctic, the CAM6 and WACCM6 sea ice
464 thickness in the Antarctic is not significantly different in the historical or PI period.

465

466 The phenology of the cloud differences between CESM2 configurations is especially
467 important for the sea ice response due to the impacts on the albedo feedback. A detailed
468 analysis of the CESM2 Arctic clouds is being completed by McIlhattan et al. (2019), and
469 we focus on only the cloud differences in CAM6 and WACCM6 that drive differences in
470 sea ice state. Previous observational and modeling studies have shown that from
471 approximately May/June through September the clouds and sea ice decouple due to the
472 relatively high static stability and low air-sea temperature gradients and during this time
473 the clouds drives the sea ice (Kay & Gettelman, 2009; Morrison et al., 2018; Morrison et
474 al., 2019; Huang et al., 2019). While there are not shortwave radiative impacts during

polar night, the longwave radiative impact could affect the surface. However, during winter months, when there is active coupling between the clouds and sea-ice, the differences in clouds between CAM6 and WACCM6 are small and contribute little to differences in the sea ice mass budget. Near surface liquid water clouds are known to dominate cloud radiative impacts in the Arctic (Morrison et al., 2018; Shupe & Intrieri, 2004). In early spring the sea ice in the CAM6 experiments experiences up to 16 Wm^{-2} more incoming shortwave radiation (and up to 8 Wm^{-2} less incoming longwave radiation) than the WACCM6 experiments. The modeled cloud fraction is fairly similar between experiments, but through the melt season there is significantly more liquid water in the WACCM6 clouds than in CAM6 indicating thicker cloud cover. The differences in incoming radiation and liquid cloud are largest in early spring (May/June) when there is not yet a large difference in sea ice fraction and around when the clouds become uncoupled from the sea ice below. While there are differences in the cloud shortwave forcing throughout the melt season, it is the impact of the early springtime forcing that initiate differences in snow and ice melt, which sets off an albedo-feedback. As the thinner ice in the CAM6 configuration melts slightly earlier, the area of ocean covered by sea ice decreases and dark ocean water is exposed, leading to increased absorption of incoming shortwave radiation that in turn heats the ocean waters and increases the ability to melt sea ice from below exposing more ocean (Perovich et al., 2007). Ultimately this leads to less summer ice cover in CAM6, less ice persisting through the year, and a thinner mean sea ice pack throughout the Arctic Basin. The spatial differences in LWP during the melt season are centered over sea ice covered regions while the IWP difference is more hemispherically uniform. Because the clouds and sea ice are decouple

498 in these months the processes constraining the large differences in LWP to be over sea
499 ice would not be driven by surface fluxes, and further in-situ observations of the coupling
500 between clouds, aerosols, and sea ice could better pin down possible mechanisms.

501

502 The two CESM2 configurations analyzed share identical atmospheric dynamical cores,
503 identical resolution for the atmosphere, ocean, and sea ice, and identical parameterization
504 tuning for these same components. Additionally, the WACCM6 experiments provide the
505 forcing for CAM6 experiments. We were surprised to find that the mean Arctic sea ice
506 state differs significantly while there is little difference in Antarctic sea ice. The
507 fundamental difference in the CESM2 configurations driving differences in the Arctic
508 clouds is the inclusion of interactive chemistry and prognostic aerosols in WACCM6.
509 Similar differences in aerosols and cloud forcings were found in WACCM6 experiments
510 with a simplified SOA parameterization as used in CAM6 (Tilmes et al., 2019). Of
511 particular importance are differences in the formation of SOA over source regions as the
512 result of the comprehensive SOA parameterization in WACCM6. This results in changes
513 in POM, BC, and sulfate aerosol reaching high northern latitudes through long-range
514 transport. Because the relative aerosol differences exist in both the PI and present-day
515 conditions, the differences in CCN production between CAM6 and WACCM6 do not
516 depend strongly on transient greenhouse gas forcing. Thus, we expect similar differences
517 in the Arctic sea ice state between CAM6 and WACCM6 in both the historical and future
518 scenario experiments. In the WACCM6 configuration more aerosols are transported to
519 the Arctic that are available as CCN for cloud droplet formation. In the more pristine
520 Antarctic, there is not a significant difference in the mean sea ice state or mass budgets,

521 which may be because there is not a difference in aerosol transport to the region. Future
522 work should analyze the transport mechanisms and pathways of these aerosols to
523 determine possible extra-polar source regions that may be impacting Arctic clouds, which
524 then in turn force the sea ice below. Credibly simulating polar cloud processes, including
525 understanding the aerosol transport into the polar regions, is essential for realistic and
526 believable historical and future climate projections of sea ice cover in both poles.

527

528 **7 Model and Data Availability**

529 Previous and current CESM versions are freely available
530 (www.cesm.ucar.edu:/models/cesm2). The CESM2 data analyzed in this manuscript have
531 been contributed to CMIP6 and are freely available at the Earth System Grid Federation
532 (ESGF; https://esgf-node.llnl.gov/search/cmip6/) or from the NCAR Digital Asset
533 Services Hub (DASH; https://data.ucar.edu) or from the links provided from the CESM
534 website (www.cesm.ucar.edu) The scripts used for this analysis in this paper can be
535 found at: https://github.com/duvivier/CESM2_sea_ice_JGR_2019

536

537 **8 Acknowledgements**

538 The CESM project is supported primarily by the National Science Foundation (NSF).
539 This material is based upon work supported by the National Center for Atmospheric
540 Research (NCAR), which is a major facility sponsored by the NSF under Cooperative
541 Agreement No.1852977. Computing and data storage resources, including the Cheyenne
542 supercomputer (doi:10.5065/D6RX99HX), were provided by the Computational and
543 Information Systems Laboratory (CISL) at NCAR. We thank all the scientists, software

544 engineers, and administrators who contributed to the development of CESM2. J. E. Kay
545 was supported by NSF CAREER (AGS #1554659). M. M. Holland acknowledges
546 support from NSF #1724748.
547
548

549 **Figures and Tables**

		CAM6 (yr. 100-1200)	CAM6 (yr. 100-500)	WACCM6 (yr. 100-500)
Surface Temperature (K)	Global	**278.3** (**1.6**)	278.2 (1.6)	278.1 (1.7)
	Northern Hemisphere	**257.5** (**11.7**)	257.3 (11.8)	257.3 (12.0)
	Southern Hemisphere	**252.6** (**6.5**)	252.5 (6.5)	252.4 (6.5)
Sea Ice Extent (10^6 km^2)	Northern Hemisphere	**12.0** (**0.30**)	**12.1** (0.30)	12.3 (0.27)
	Southern Hemisphere	**13.1** (**0.48**)	13.6 (0.46)	13.5 (0.44)
Sea Ice Volume (10^3 km^3)	Northern Hemisphere	**22.3** (1.96)	**23.1** (1.96)	27.0 (1.93)
	Southern Hemisphere	**14.1** (0.91)	**14.5** (0.89)	14.2 (0.84)

550

551 **Table 1**: CAM6 and WACCM6 hemispheric annual mean and standard deviation, in
552 parenthesis, surface temperature (K), sea ice extent (10^6 km^2), and sea ice volume (10^3
553 km^3). Means were calculated from the PI experiment over the years listed. Bold values in
554 the CAM6 columns indicate when the means (standard deviation) as determined by a
555 Welch's t-test (F-test) are significantly different at the 95% level from the WACCM6
556 values.

		CAM6 PI (historical)	WACCM6 PI (historical)	Historical Data
Sea Ice Extent Trend (10^6 km^2/century)	Northern Hemisphere	-0.031 (-5.3)	-0.063 (-5.2)	-5.3
	Southern Hemisphere	-0.067 (-4.1)	-0.11 (-5.6)	+2.0
Sea Ice Volume Trend (10^3 km^3/century)	Northern Hemisphere	-0.20 (-27.2)	-0.31 (-48.2)	-25.0 (-30.3)
	Southern Hemisphere	-0.13 (-6.8)	-0.15 (-8.6)	+5.5

Table 2: Hemispheric trends in annual mean sea ice extent (10^6 km^2/century) and sea ice volume (10^3 km^3/century) for CAM6 and WACCM6 ensemble mean during the PI and, in parenthesis, historical periods. The PI trends were calculated over years 100-1200 (100-500) for CAM6 (WACCM6), and the historical trends are calculated for 1979-2014. The right column shows the historical trend in sea ice extent from the NSIDC sea ice index (Fetterer et al., 2017). The historical trend in reconstructed sea ice volume for GIOMAS (Zhang and Rothrock, 2003) is shown for both hemispheres and, for the Northern Hemisphere, PIOMAS (Schweiger et al., 2011) is shown in parenthesis.

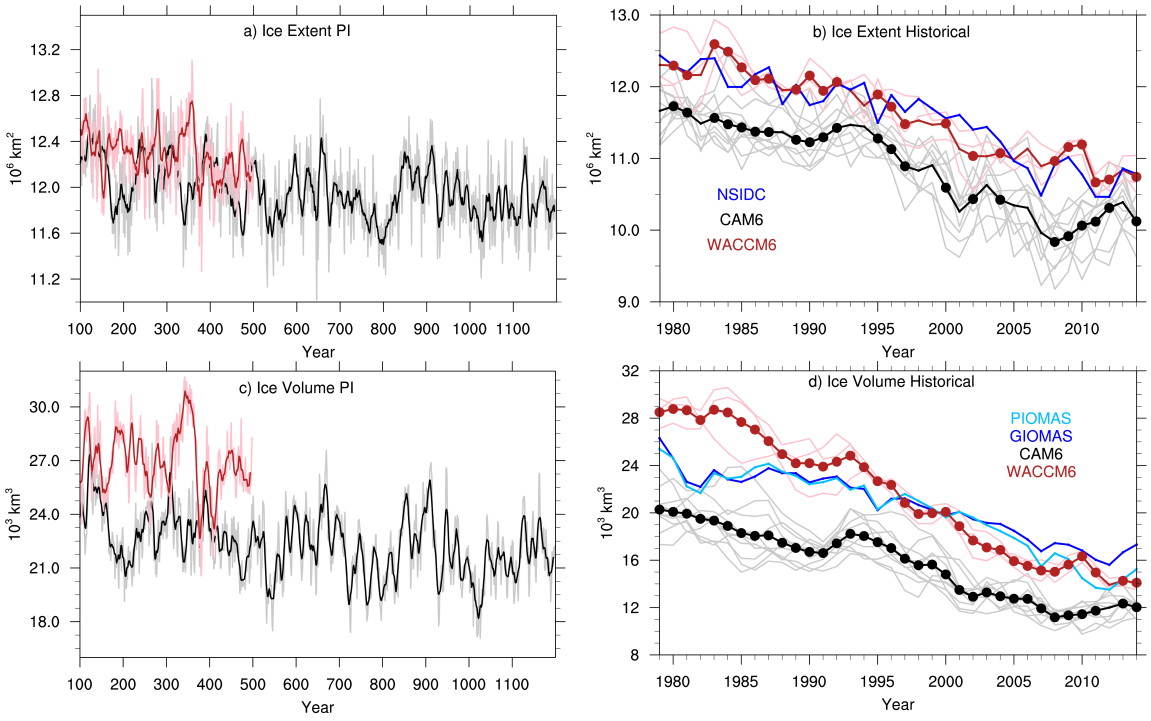

Figure 1: Time series of annual mean Northern Hemispheric (a), (b) sea ice extent (10^6 km^2) and (c), (d) sea ice volume (10^3 km^3) for the (a),(c) PI and (b),(d) historical time periods. In (a),(c), the 10-year running mean and raw annual values are shown for CAM6 (black and grey, respectively) and WACCM6 (red and pink, respectively). In (b),(d) individual ensembles and ensemble mean are shown for CAM6 (grey and black, respectively) and WACCM6 (pink and red, respectively), and large solid circles indicate years in which the CAM6 and WACCM6 ensemble means are different at the 95% significance level. In (b) the NSIDC sea ice index (Fetterer et al., 2017) is shown in blue. In (d) the reconstructed sea ice volume for PIOMAS (Schweiger et al., 2011) and GIOMAS (Zhang and Rothrock, 2003) are shown in light blue and dark blue respectively.

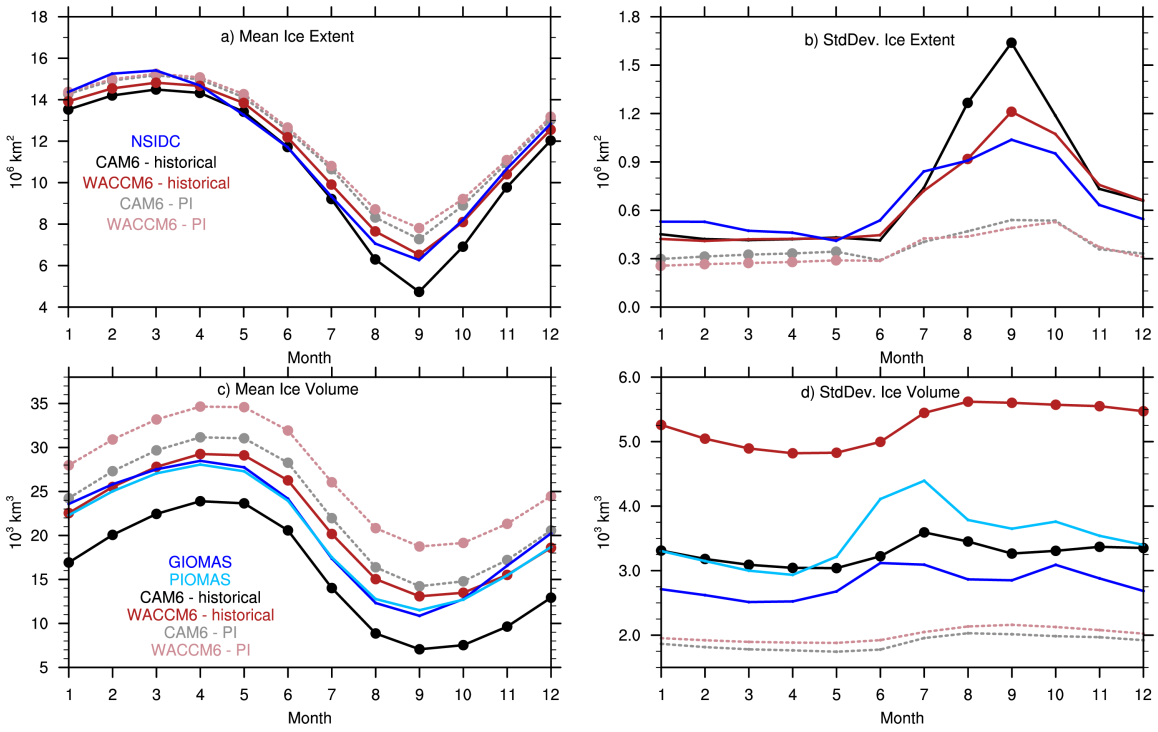

578

579 **Figure 2**: Northern Hemispheric annual cycle of (a), (b) sea ice extent (10^6 km^2) and (c),
580 (d) sea ice volume (10^3 km^3) for the (a),(c) mean and (b),(d) standard deviation. The PI
581 statistics are calculated over years 100-500, and historical statistics are calculated for
582 1979-2014 and all ensemble members. Large solid circles indicate months in which the
583 CAM6 and WACCM6 ensemble means are different at the 95% significance level. In
584 (b),(c) the NSIDC sea ice index (Fetterer et al., 2017) is shown in blue. In (c),(d) the
585 reconstructed sea ice volume for PIOMAS (Schweiger et al., 2011) and GIOMAS (Zhang
586 and Rothrock, 2003) are shown in light blue and dark blue respectively.

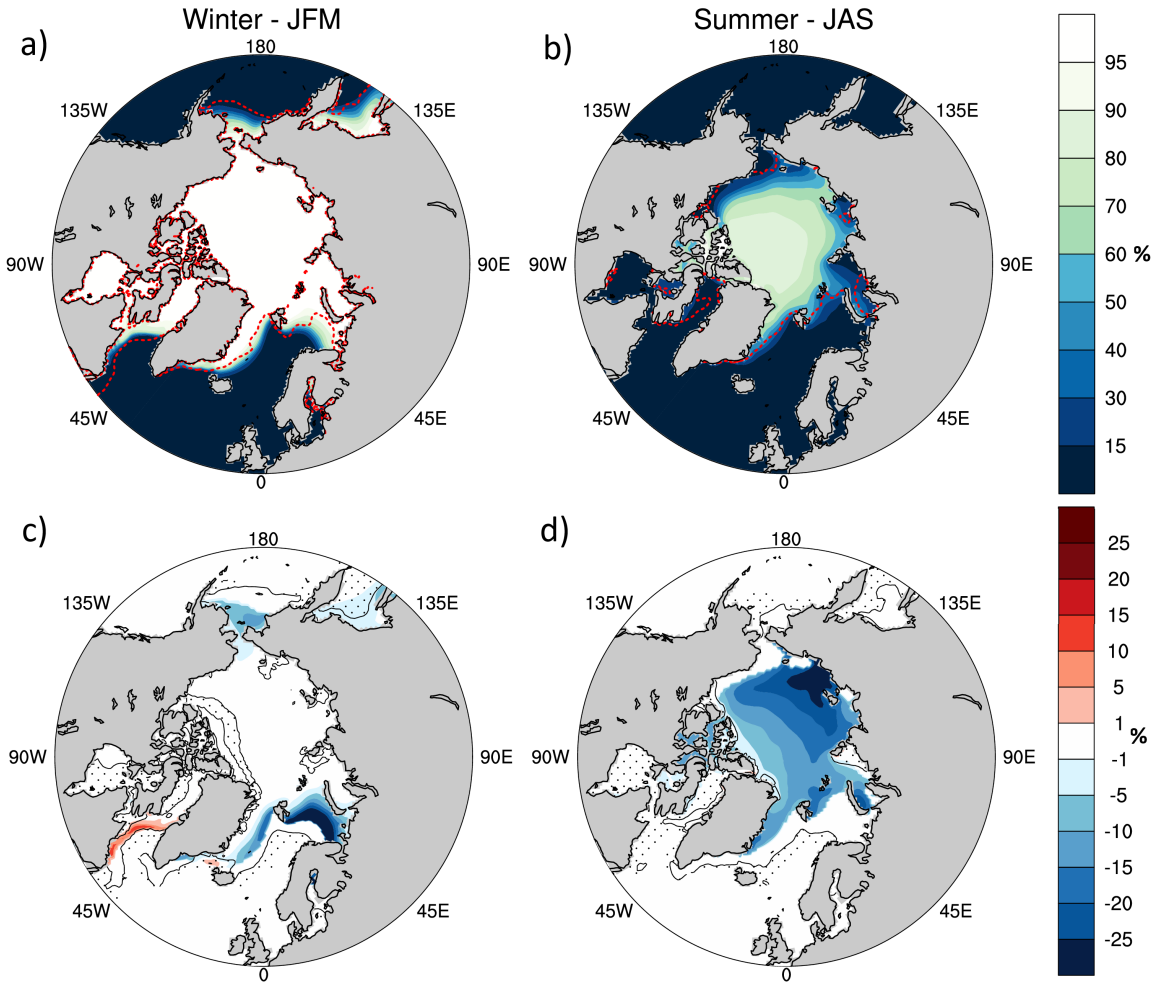

587

588 **Figure 3**: Arctic historical (1979-2014) ensemble mean sea ice concentration (%) for
589 (a),(b) WACCM6 and (c),(d) difference (CAM6-WACCM6) in winter (January-March)
590 and summer (July-September) months. Stippling indicates locations where the CAM6
591 and WACCM6 values are not different at the 95% significance level. The observed sea
592 ice edge (Comiso, 2000; concentration <15%) is shown in red on (a) and (b).

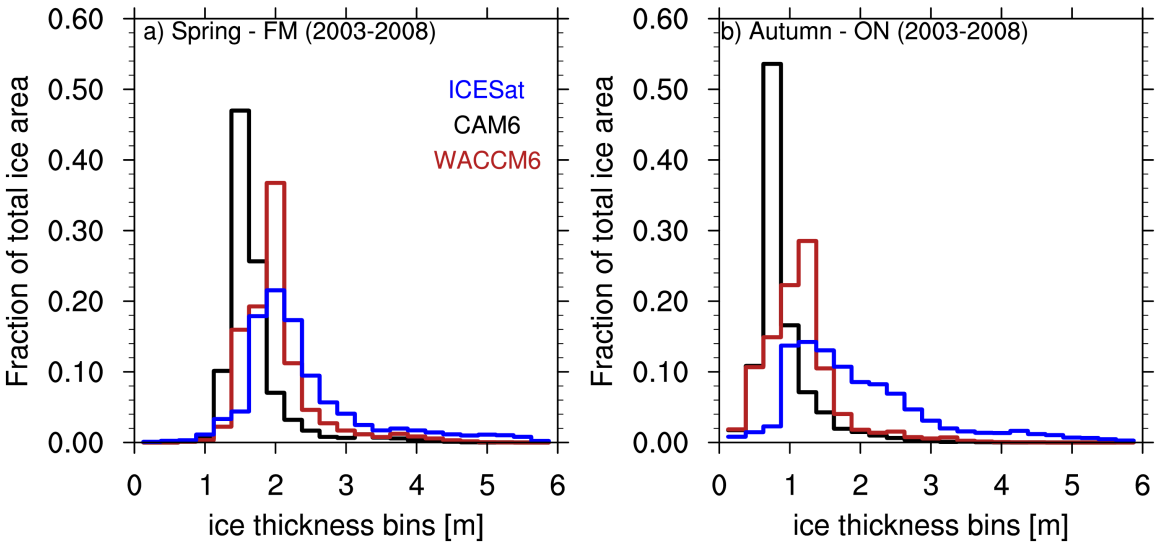

593

594 **Figure 4**: Histogram of the sea ice thickness (m) distribution in the Arctic Ocean for (a)
595 spring (February-March) and (b) autumn (October-November) normalized by the fraction
596 of the total ice area covered. The ICESat data (Kwok et al. 2009; blue) are averaged over
597 fall 2004-2008 and spring 2003-2007, while the CAM6 (black) and WACCM6 (red) data
598 are averaged over 2003-2008 for both spring and autumn and only over the central Arctic
599 Ocean where ICESat data are co-located (See Figure 5).

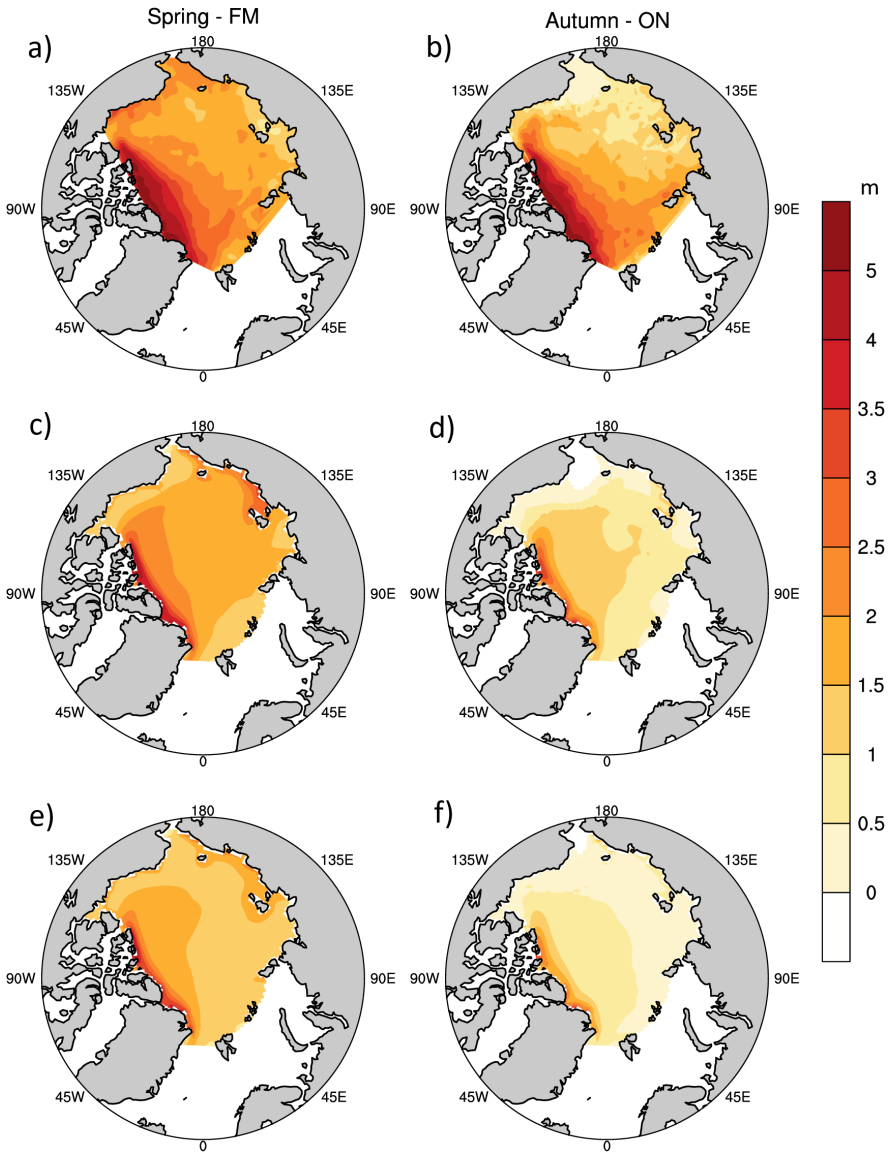

Figure 5: Sea ice thickness (m) from (a),(b) ICESat data (Kwok et al. 2009), (b),(c) WACCM6, and (d),(e) CAM6 for (left) Spring (February-March) and (right) Fall (October-November). The ICESat data are averaged over fall 2004-2008 and spring 2003-2007, while the WACCM6 and CAM6 data are averaged over 2003-2008 for both spring and fall. The WACCM6 and CAM6 ensemble averages of all available members are shown in panels (b)-(d) and show only the regions with co-located ICESat data.

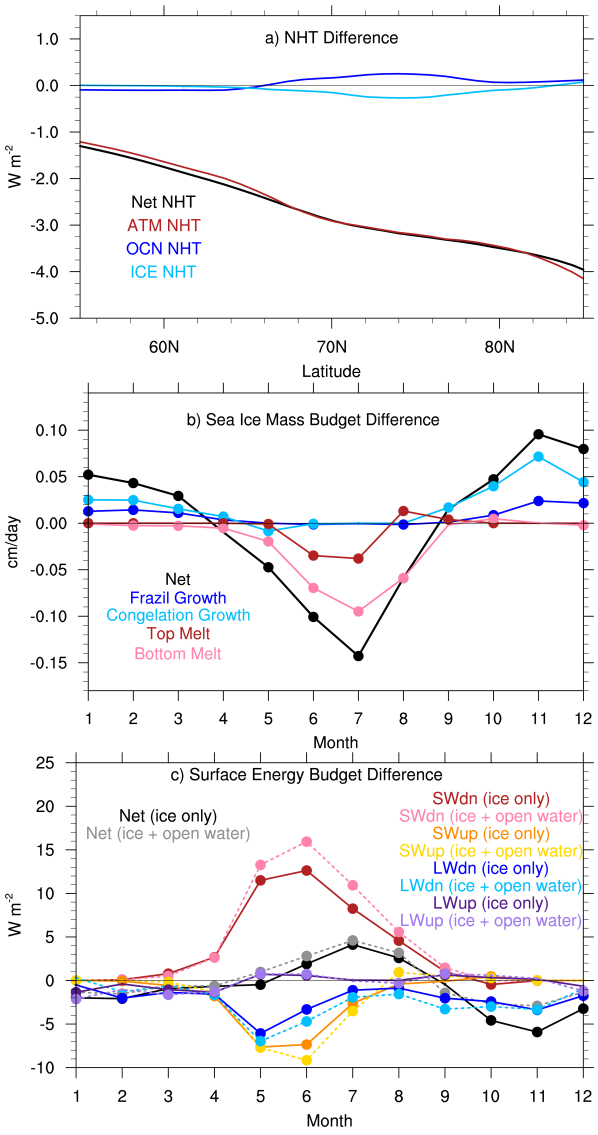

607

608 **Figure 6**: Difference (CAM6-WACCM6) in (a) zonal mean northward heat transport

609 divided by the surface area north of the given latitude (W m^{-2}) and component terms, (b)

610 net sea ice mass budget (cm day^{-1}) and component terms, and (c) net surface energy

611 budget (W m^{-2}) and radiative component terms over sea ice only (solid; dark colors) and

612 over the ocean and ice surface (dashed; light colors). In (b),(c) large solid circles indicate

613 when the CAM6 and WACCM6 values are different at the 95% significance level. The

614 CAM6 and WACCM6 means are calculated over the PI years 100-500.

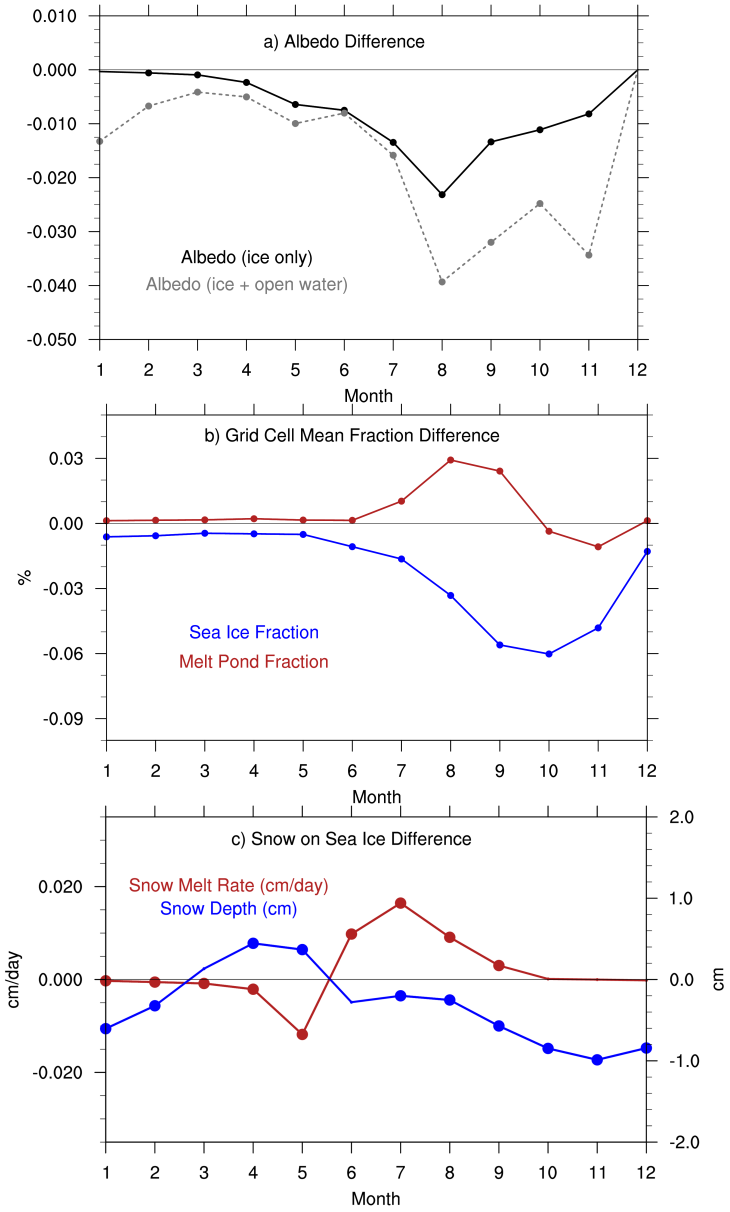

615

616 **Figure 7**: Monthly mean difference (CAM6-WACCM6) in (a) surface albedo over sea
617 ice only (solid; black) and over the whole surface (dashed; grey), (b) fraction (%) of grid
618 cell covered by sea ice (blue) and melt ponds (red), and (c) the melt rate for snow on sea
619 ice (red; cm/day) and depth of snow on sea ice (blue; cm). Large solid circles indicate
620 when the CAM6 and WACCM6 values are different at the 95% significance level. The
621 CAM6 and WACCM6 means are calculated over the PI years 100-500.

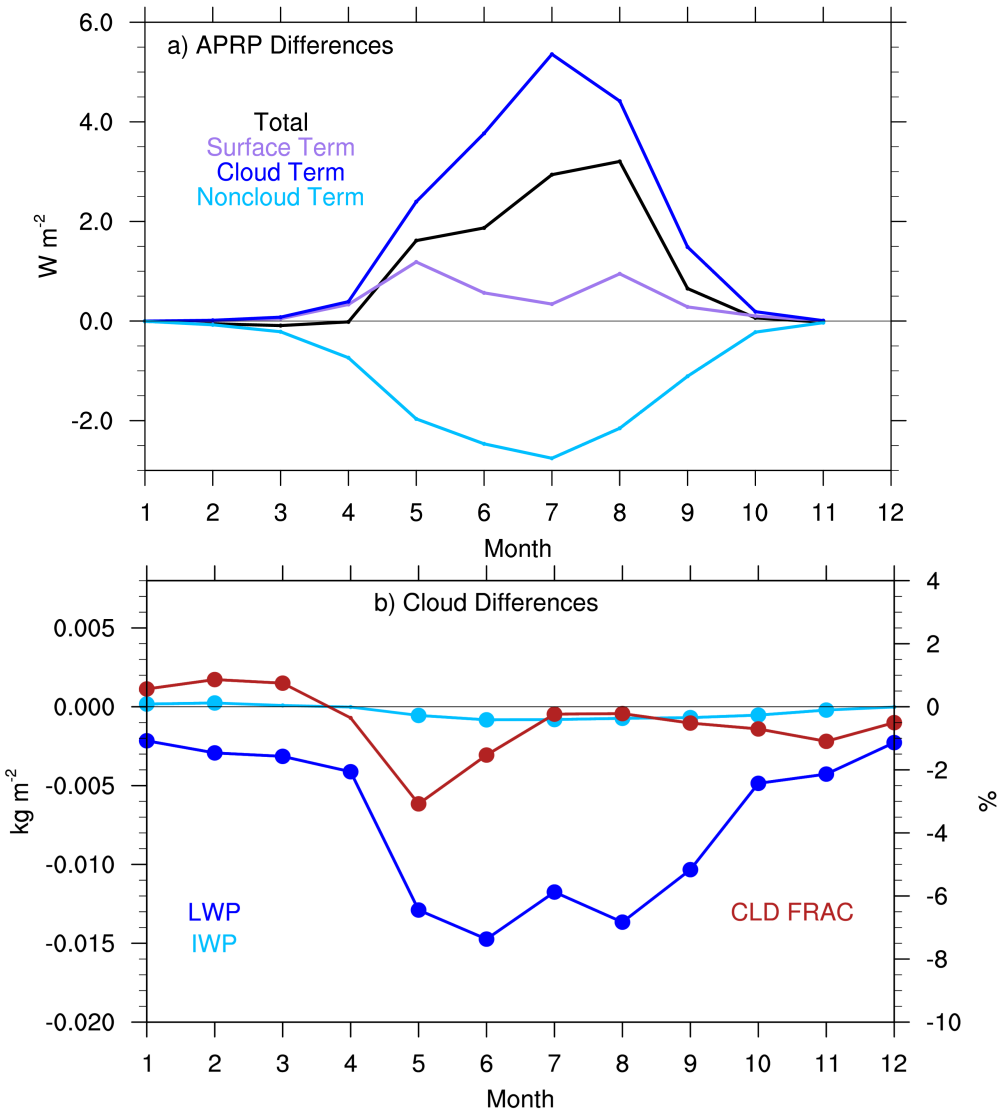

622

623 **Figure 8**: Monthly mean difference (CAM6-WACCM6) over 70-90°N for (a) mean

624 APRP shortwave feedback terms (W m^{-2}) and (b) cloud fraction (%) and cloud liquid

625 water path and ice water path (kg m^{-2}). Large solid circles indicate when the CAM6 and

626 WACCM6 values are different at the 95% significance level. The CAM6 and WACCM6

627 means are calculated over the PI years 100-500.

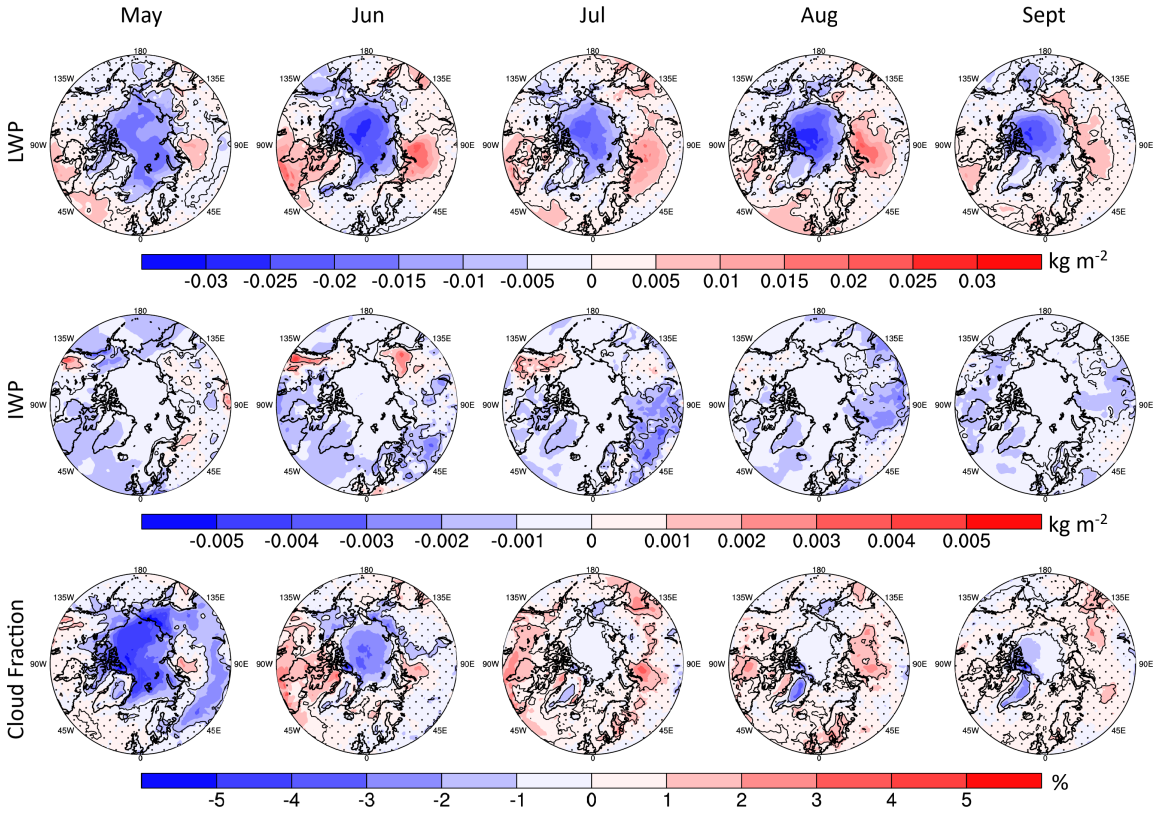

Figure 9. Monthly mean difference (CAM6-WACCM6) for (top row) cloud LWP (kg m^{-2}), (middle row) cloud IWP (kg m^{-2}), and (bottom row) cloud fraction (%) for the months of May, June, July, August, and September. Stippling indicates locations where the CAM6 and WACCM6 values are not different at the 95% significance level. The CAM6 and WACCM6 means are calculated over the PI years 100-500.

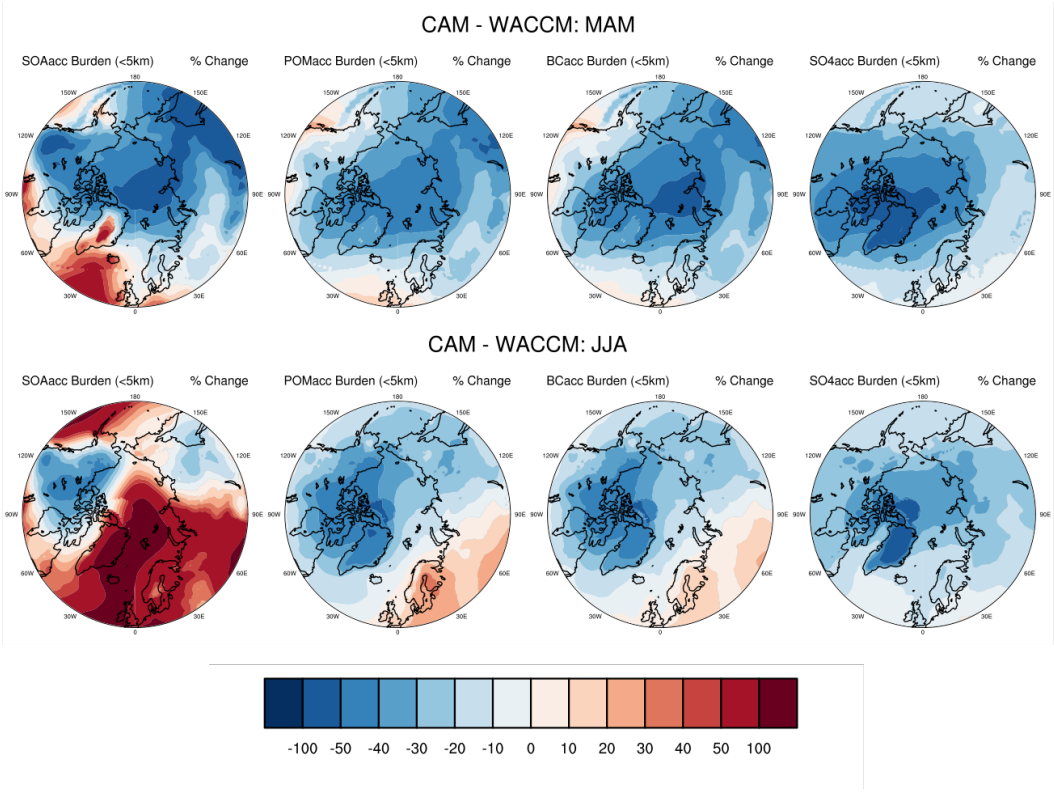

635

636 **Figure 10**: Percent change in (CAM6-WACCM6) Arctic aerosol burden for (top row)
637 spring (March-May) and (bottom row) summer (June-August). Aerosols shown are (left
638 column) Secondary Organic Aerosols, (left-middle column) Primary Organic Matter,
639 (right-middle column) Black Carbon, and (right column) Sulfates.

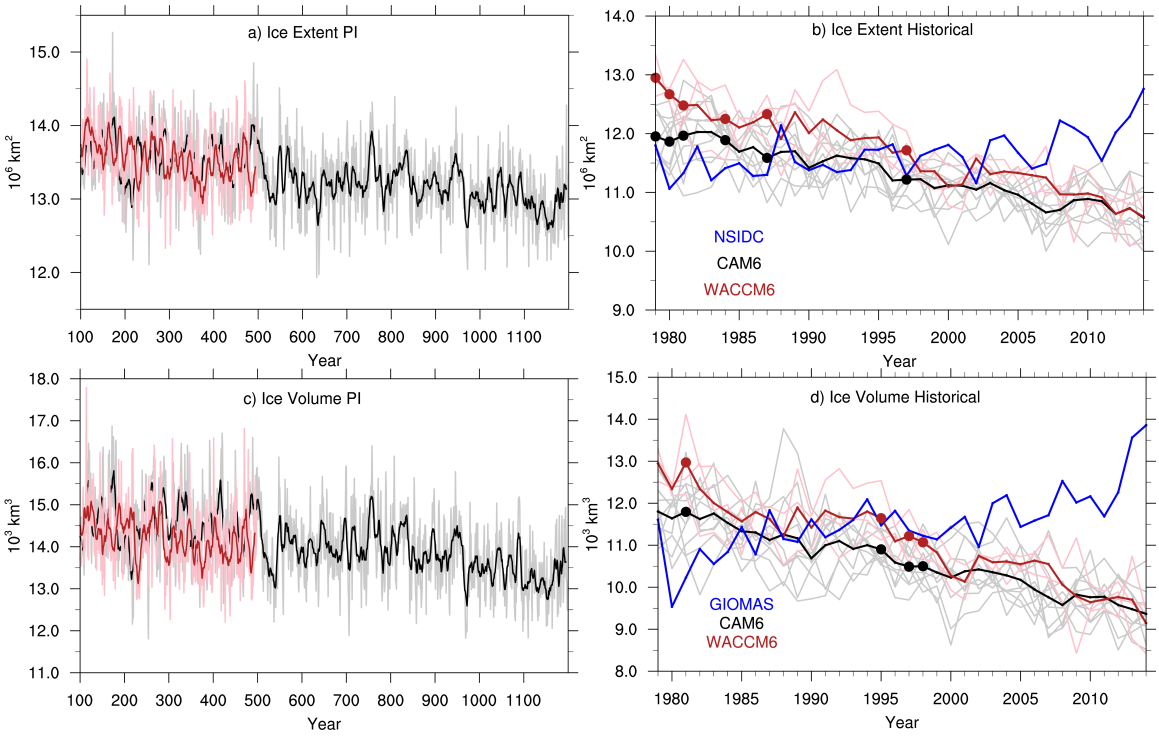

640

641 **Figure 11**: As in Figure 1, but for the Southern Hemisphere.

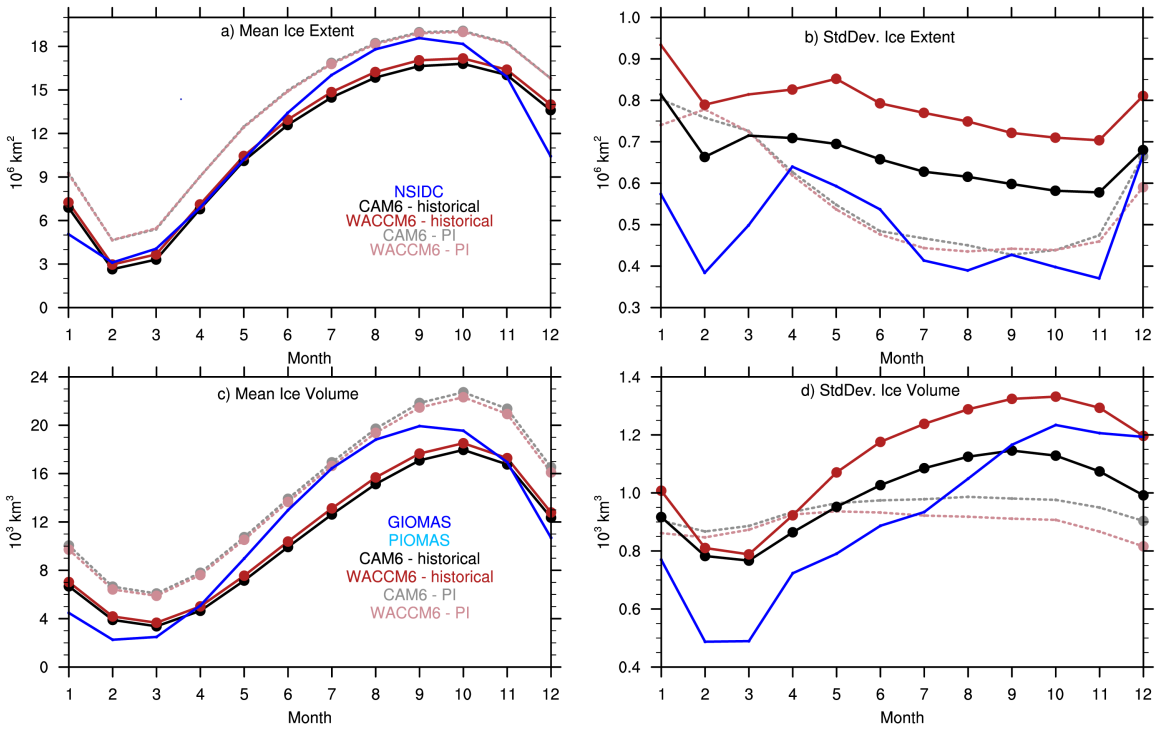

642

643 **Figure 12**: As in Figure 2, but for the Southern Hemisphere.

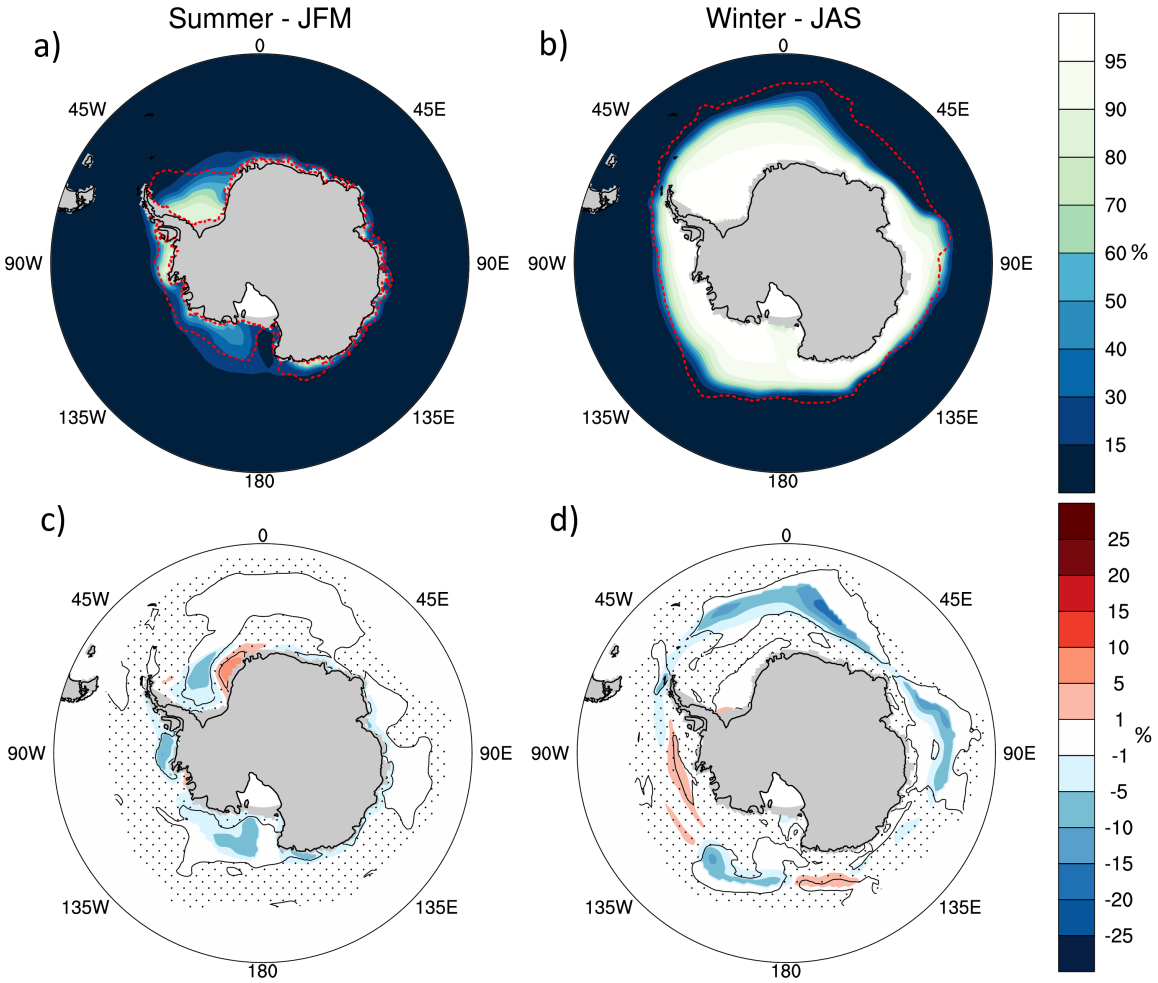

644

645 **Figure 13**: As in Figure 3, but for the Southern Hemisphere.

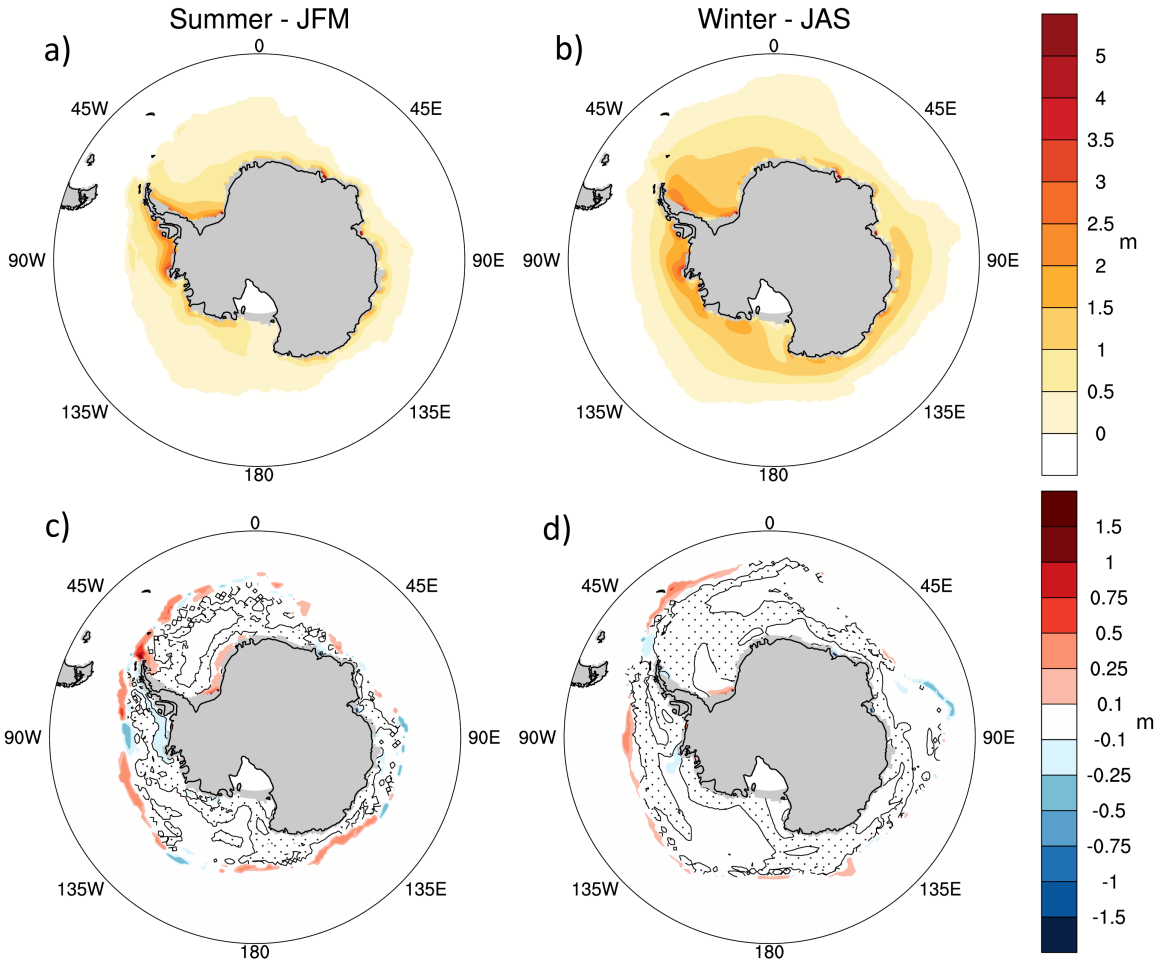

646

647 **Figure 14**: Antarctic historical (1979-2014) ensemble mean sea ice thickness (m) for

648 (a),(b) WACCM6 and (c),(d) difference (CAM6-WACCM6) in summer (January-March)

649 and winter (July-September) months. Stippling indicates locations where the CAM6 and

650 WACCM6 values are not different at the 95% significance level.

651

652 **References**

653 Alexander, M. A. (2004). The Atmospheric Response to Realistic Arctic Sea Ice
654 Anomalies in an AGCM during Winter. *JOURNAL OF CLIMATE*, *17*, 16.
655 https://doi.org/10.1175/1520-0442(2004)017<0890:TARTRA>2.0.CO;2

656 Bailey, D. A., Holland, M. M., DuVivier, A. K., Hunke, E. C., & Turner, A. K. (2019).
657 Impact of Sea Ice Thermodynamics in the CESM2 sea ice component. *Journal of*
658 *Geophysical Research: Ocean*.

659 Barnes, E. A., & Screen, J. A. (2015). The impact of Arctic warming on the midlatitude
660 jet-stream: Can it? Has it? Will it? *Wiley Interdisciplinary Reviews: Climate*
661 *Change*, *6*(3), 277–286. https://doi.org/10.1002/wcc.337

662 Barnhart, K. R., Miller, C. R., Overeem, I., & Kay, J. E. (2015). Mapping the future
663 expansion of Arctic open water. *Nature Climate Change*, *6*(3), 280–285.
664 https://doi.org/10.1038/nclimate2848

665 Bitz, C. M., Holland, M. M., Hunke, E. C., & Moritz, R. E. (2005). Maintenance of the
666 Sea-Ice Edge. *Journal of Climate*, *18*(15), 2903–2921.
667 https://doi.org/10.1175/JCLI3428.1

668 Boisvert, L. N., & Stroeve, J. C. (2015). The Arctic is becoming warmer and wetter as
669 revealed by the Atmospheric Infrared Sounder. *Geophysical Research Letters*,
670 *42*(11), 4439–4446. https://doi.org/10.1002/2015GL063775

671 Comiso, J. C. (2000). Bootstrap sea ice concentrations from Nimbus-7 SSMR and DMSP
672 SSM/I-SSMIS, version 2. Boulder, Colorado USA: National Snow and Ice Data
673 Center. Digital media. Retrieved from http://nsidc.org/data/nsidc-0079

674 Danabasoglu, G., Bates, S. C., Briegleb, B. P., Jayne, S. R., Jochum, M., Large, W. G., et
675 al. (2012). The CCSM4 Ocean Component. *Journal of Climate*, *25*(5), 1361–
676 1389. https://doi.org/10.1175/JCLI-D-11-00091.1
677 Danabasoglu, G., Lamarque, J.-F., Bachmeister, J., Bailey, D. A., DuVivier, A. K.,
678 Edwards, J., et al. (2019). The Community Earth System Model version 2
679 (CESM2). *Journal of Advances in Modeling Earth Systems*.
680 DeRepentigny, P., Tremblay, L. B., Newton, R., & Pfirman, S. (2016). Patterns of Sea
681 Ice Retreat in the Transition to a Seasonally Ice-Free Arctic. *Journal of Climate*,
682 *29*(19), 6993–7008. https://doi.org/10.1175/JCLI-D-15-0733.1
683 Deser, C., Sun, L., Tomas, R. A., & Screen, J. (2016). Does ocean coupling matter for the
684 northern extratropical response to projected Arctic sea ice loss? *Geophysical*
685 *Research Letters*, *43*(5), 2149–2157. https://doi.org/10.1002/2016GL067792
686 Fetterer, F., Knowles, K., Meier, W. N., Savoie, M. H., & Windnagel, A. K. (2017). Sea
687 Ice Index, Version 3. *NSIDC: National Snow and Ice Data Center. Boulder,*
688 *Colorado USA*. https://doi.org/10.7265/N5K072F8
689 Gettelman, A., Mills, M. J., Kinnison, D., Garcia, R., Smith, A., Marsh, D., et al. (2019).
690 The Whole Atmosphere Community Climate Model Version 6 (WACCM6).
691 *Journal of Geophysical Research-Atmospheres*.
692 Goosse, H., Arzel, O., Bitz, C. M., de Montety, A., & Vancoppenolle, M. (2009).
693 Increased variability of the Arctic summer ice extent in a warmer climate.
694 *Geophysical Research Letters*, *36*(23), L23702.
695 https://doi.org/10.1029/2009GL040546

696 Goosse, Hugues, Kay, J. E., Armour, K. C., Bodas-Salcedo, A., Chepfer, H., Docquier,
697 D., et al. (2018). Quantifying climate feedbacks in polar regions. *Nature*
698 *Communications*, *9*(1), 1919. https://doi.org/10.1038/s41467-018-04173-0
699 Hobbs, W. R., Bindoff, N. L., & Raphael, M. N. (2015). New perspectives on observed
700 and simulated Antarctic Sea ice extent trends using optimal fingerprinting
701 techniques. *Journal of Climate*, *28*(4), 1543–1560.
702 Holland, M. M., Bitz, C. M., Hunke, E. C., Lipscomb, W. H., & Schramm, J. L. (2006).
703 Influence of the Sea Ice Thickness Distribution on Polar Climate in CCSM3.
704 *Journal of Climate*, *19*(11), 2398–2414. https://doi.org/10.1175/JCLI3751.1
705 Holland, M. M., Bitz, C. M., Tremblay, L.-B., & Bailey, D. A. (2008). The Role of
706 Natural Versus Forced Change in Future Rapid Summer Arctic Ice Loss. In E. T.
707 DeWeaver, C. M. Bitz, & L.-B. Tremblay (Eds.), *Geophysical Monograph Series*
708 (pp. 133–150). Washington, D.C.: American Geophysical Union.
709 https://doi.org/10.1029/180GM10
710 Huang, Y., Dong, X., Bailey, D. A., Holland, M. M., Xi, B., DuVivier, A. K., et al.
711 (2019). Thicker clouds and accelerated Arctic sea ice decline: The atmosphere-sea
712 ice interactions in spring. *Geophysical Research Letters*, 2019GL082791.
713 https://doi.org/10.1029/2019GL082791
714 Hunke, E. C., Hebert, D. A., & Lecomte, O. (2013). Level-ice melt ponds in the Los
715 Alamos sea ice model, CICE. *Ocean Modelling*, *71*, 26–42.
716 https://doi.org/10.1016/j.ocemod.2012.11.008
717 Hunke, E. C., Lipscomb, W. H., Turner, A. K., Jeffery, N., & Elliott, S. (2015). CICE:
718 the Los Alamos Sea Ice Model Documentation and Software User's Manual

719 Version 5.1 LA-CC-012. Retrieved from http://oceans11.
720 lanl.gov/trac/CICE/wiki/SourceCode
721 Hunter, C. M., Caswell, H., Runge, M. C., Regehr, E. V., Amstrup, S. C., & Stirling, I.
722 (2010). Climate change threatens polar bear populations: a stochastic
723 demographic analysis, *91*(10), 15.
724 Jahn, A., Sterling, K., Holland, M. M., Kay, J. E., Maslanik, J. A., Bitz, C. M., et al.
725 (2012). Late-Twentieth-Century Simulation of Arctic Sea Ice and Ocean
726 Properties in the CCSM4. *Journal of Climate*, *25*(5), 1431–1452.
727 https://doi.org/10.1175/JCLI-D-11-00201.1
728 Jahn, A., Kay, J. E., Holland, M. M., & Hall, D. M. (2016). How predictable is the timing
729 of a summer ice-free Arctic? *Geophysical Research Letters*, *43*(17), 9113–9120.
730 https://doi.org/10.1002/2016GL070067
731 Jenouvrier, S., Holland, M., Stroeve, J., Serreze, M., Barbraud, C., Weimerskirch, H., &
732 Caswell, H. (2014). Projected continent-wide declines of the emperor penguin
733 under climate change. *NATURE CLIMATE CHANGE*, *4*, 4.
734 Kay, J. E., & Gettelman, A. (2009). Cloud influence on and response to seasonal Arctic
735 sea ice loss. *Journal of Geophysical Research*, *114*(D18).
736 https://doi.org/10.1029/2009JD011773
737 Kay, J. E., Holland, M. M., & Jahn, A. (2011a). Inter-annual to multi-decadal Arctic sea
738 ice extent trends in a warming world. *Geophysical Research Letters*, *38*(15).
739 https://doi.org/10.1029/2011GL048008
740 Kay, J. E., Raeder, K., Gettelman, A., & Anderson, J. (2011b). The Boundary Layer
741 Response to Recent Arctic Sea Ice Loss and Implications for High-Latitude

742 Climate Feedbacks. *Journal of Climate*, *24*(2), 428–447.
743 https://doi.org/10.1175/2010JCLI3651.1
744 Kay, J. E., Holland, M. M., Bitz, C. M., Blanchard-Wrigglesworth, E., Gettelman, A.,
745 Conley, A., & Bailey, D. (2012). The Influence of Local Feedbacks and
746 Northward Heat Transport on the Equilibrium Arctic Climate Response to
747 Increased Greenhouse Gas Forcing. *Journal of Climate*, *25*(16), 5433–5450.
748 https://doi.org/10.1175/JCLI-D-11-00622.1
749 Kovacs, K. M., Lydersen, C., Overland, J. E., & Moore, S. E. (2011). Impacts of
750 changing sea-ice conditions on Arctic marine mammals, 14.
751 Kwok, R. (2018). Arctic sea ice thickness, volume, and multiyear ice coverage: losses
752 and coupled variability (1958–2018). *Environmental Research Letters*, *13*(10),
753 105005. https://doi.org/10.1088/1748-9326/aae3ec
754 Kwok, R., Cunningham, G. F., Wensnahan, M., Rigor, I., Zwally, H. J., & Yi, D. (2009).
755 Thinning and volume loss of the Arctic Ocean sea ice cover: 2003–2008. *Journal*
756 *of Geophysical Research: Oceans*, *114*(C7), C07005.
757 https://doi.org/10.1029/2009JC005312
758 Labe, Z., Magnusdottir, G., & Stern, H. (2018). Variability of Arctic Sea Ice Thickness
759 Using PIOMAS and the CESM Large Ensemble. *Journal of Climate*, *31*(8),
760 3233–3247. https://doi.org/10.1175/JCLI-D-17-0436.1
761 Landrum, L., Holland, M. M., Schneider, D. P., & Hunke, E. (2012). Antarctic Sea Ice
762 Climatology, Variability, and Late Twentieth-Century Change in CCSM4.
763 *Journal of Climate*, *25*(14), 4817–4838. https://doi.org/10.1175/JCLI-D-11-
764 00289.1

765 Lindsay, R., & Schweiger, A. (2015). Arctic sea ice thickness loss determined using
766 subsurface, aircraft, and satellite observations. *The Cryosphere*, *9*(1), 269–283.
767 https://doi.org/10.5194/tc-9-269-2015
768 Liu, Y., Key, J., Wang, X., & Tschudi, Mark A. (2019). Multidecadal Arctic sea ice
769 thickness and volume derived from ice age. *The Cryosphere*.
770 https://doi.org/10.5194/tc-2019-192
771 Mahlstein, I., Gent, P. R., & Solomon, S. (2013). Historical Antarctic mean sea ice area,
772 sea ice trends, and winds in CMIP5 simulations. *Journal of Geophysical*
773 *Research: Atmospheres*, *118*(11), 5105–5110. https://doi.org/10.1002/jgrd.50443
774 Maykut, G. A. (1982). Large-scale heat exchange and ice production in the central Arctic.
775 *Journal of Geophysical Research*, *87*(C10), 7971.
776 https://doi.org/10.1029/JC087iC10p07971
777 McIlhattan, E. A., Kay, J. E., & L'Ecuyer, T. S. (2019). Arctic Clouds and Precipitation
778 in the Community Earth System Model Version 2. *Journal of Geophysical*
779 *Research: Atmospheres*.
780 Meehl, G. A., Arblaster, J. M., Chung, C. T. Y., Holland, M. M., DuVivier, A.,
781 Thompson, L., et al. (2019). Sustained ocean changes contributed to sudden
782 Antarctic sea ice retreat in late 2016. *Nature Communications*, *10*(1).
783 https://doi.org/10.1038/s41467-018-07865-9
784 Meredith, M., & Sommerkorn, M. (2019). Chapter 3: Polar Regions. In *IPCC Special*
785 *Report on the Ocean and Cryosphere in a Changing Climate*.
786 Mills, M. J., Richter, J. H., Tilmes, S., Kravitz, B., MacMartin, D. G., Glanville, A. A., et
787 al. (2017). Radiative and Chemical Response to Interactive Stratospheric Sulfate

788 Aerosols in Fully Coupled CESM1(WACCM). *Journal of Geophysical Research:*
789 *Atmospheres*, *122*(23), 13,061-13,078. https://doi.org/10.1002/2017JD027006
790 Moon, T. A., Overeem, I., Druckenmiller, M., Holland, M., Huntington, H., Kling, G., et
791 al. (2019). The Expanding Footprint of Rapid Arctic Change. *Earth's Future*,
792 *7*(3), 212–218. https://doi.org/10.1029/2018EF001088
793 Morrison, A., Kay, J. E., Chepfer, H., Guzman, R., & Yettella, V. (2018). Isolating the
794 Liquid Cloud Response to Recent Arctic Sea Ice Variability Using Spaceborne
795 Lidar Observations. *Journal of Geophysical Research: Atmospheres*, *123*(1), 473–
796 490. https://doi.org/10.1002/2017JD027248
797 Morrison, A., Kay, J. E., Frey, W. R., Chepfer, H., & Guzman, R. (2019). Cloud
798 Response to Arctic Sea Ice Loss and Implications for Future Feedbacks in the
799 CESM1 Climate Model. *Journal of Geophysical Research: Atmospheres*.
800 https://doi.org/10.1029/2018JD029142
801 Neale, R. B., & co-authors. (2019). The NCAR Community Atmosphere Model version 6
802 (CAM6): Scientific configuration and simulation fidelity. *Journal of Advances in*
803 *Modeling Earth Systems*.
804 Notz, D., Jahn, A., Holland, M., Hunke, E., Massonnet, F., Stroeve, J., et al. (2016). The
805 CMIP6 Sea-Ice Model Intercomparison Project (SIMIP): understanding sea ice
806 through climate-model simulations. *Geoscientific Model Development*, *9*(9),
807 3427–3446. https://doi.org/10.5194/gmd-9-3427-2016
808 Parkinson, C. L. (2014). Global Sea Ice Coverage from Satellite Data: Annual Cycle and
809 35-Yr Trends. *Journal of Climate*, *27*(24), 9377–9382.
810 https://doi.org/10.1175/JCLI-D-14-00605.1

811 Perovich, D. K., Light, B., Eicken, H., Jones, K. F., Runciman, K., & Nghiem, S. V.
812 (2007). Increasing solar heating of the Arctic Ocean and adjacent seas, 1979–
813 2005: Attribution and role in the ice-albedo feedback. *Geophysical Research*
814 *Letters*, *34*(19), L19505. https://doi.org/10.1029/2007GL031480
815 Pithan, F., & Mauritsen, T. (2014). Arctic amplification dominated by temperature
816 feedbacks in contemporary climate models. *Nature Geoscience*, *7*(3), 181–184.
817 https://doi.org/10.1038/ngeo2071
818 Richter-Menge, J. A., Osborne, E., Druckenmiller, M., & Jeffries, M. O. (Eds.). (2019).
819 The Arctic [in "State of the Climate in 2018"]. *Bulletin of the American*
820 *Meteorological Society*, *100*(9), S141–S168.
821 Schweiger, A., Lindsay, R., Zhang, J., Steele, M., Stern, H., & Kwok, R. (2011).
822 Uncertainty in modeled Arctic sea ice volume. *Journal of Geophysical Research*,
823 *116*, C00D06. https://doi.org/10.1029/2011JC007084
824 Shupe, M. D., & Intrieri, J. M. (2004). Cloud radiative forcing of the Arctic surface: The
825 influence of cloud properties, surface albedo, and solar zenith angle. *Journal of*
826 *Climate*, *17*(3), 616–628. http://dx.doi.org/10.1175/1520-
827 0442(2004)017<0616:CRFOTA>2.0.CO;2
828 Smith, R., Jones, P., Briegleb, B., Bryan, F., Danabasoglu, G., Dennis, J., et al. (2010).
829 The Parallel Ocean Program (POP) Reference Manual Ocean Component of the
830 Community Climate System Model (CCSM) and Community Earth System
831 Model (CESM). *Rep. LAUR-01853*, *141*. Retrieved from
832 https://ccsm.ucar.edu/models/cesm1.2/pop2/doc/sci/POPRefManual.pdf

833 Stroeve, J., & Notz, D. (2018). Changing state of Arctic sea ice across all seasons.
834 *Environmental Research Letters*, *13*(10), 103001. https://doi.org/10.1088/1748-
835 9326/aade56
836 Stuecker, M. F., Bitz, C. M., & Armour, K. C. (2017). Conditions leading to the
837 unprecedented low Antarctic sea ice extent during the 2016 austral spring season.
838 *Geophysical Research Letters*. https://doi.org/10.1002/2017GL074691
839 Swart, N. C., Fyfe, J. C., Hawkins, E., Kay, J. E., & Jahn, A. (2015). Influence of internal
840 variability on Arctic sea-ice trends. *Nature Climate Change*, *5*(2), 86–89.
841 https://doi.org/10.1038/nclimate2483
842 Taylor, K. E., Crucifix, M., Braconnot, P., Hewitt, C. D., Doutriaux, C., Broccoli, A. J.,
843 et al. (2007). Estimating Shortwave Radiative Forcing and Response in Climate
844 Models. *Journal of Climate*, *20*(11), 2530–2543.
845 https://doi.org/10.1175/JCLI4143.1
846 Tilmes, S., Hodzic, A., Emmons, L. K., & et al. (2019). Climate forcing and trends of
847 organic aerosols in the Community Earth System Model (CESM2). *Journal of*
848 *Advances in Modeling Earth Systems*.
849 Turner, A. K., & Hunke, E. C. (2015). Impacts of a mushy-layer thermodynamic
850 approach in global sea-ice simulations using the CICE sea-ice model. *Journal of*
851 *Geophysical Research: Oceans*, *120*(2), 1253–1275.
852 https://doi.org/10.1002/2014JC010358
853 Turner, J., Phillips, T., Marshall, G. J., Hosking, J. S., Pope, J. O., Bracegirdle, T. J., &
854 Deb, P. (2017). Unprecedented springtime retreat of Antarctic sea ice in 2016:

The 2016 Antarctic Sea Ice Retreat. *Geophysical Research Letters*, *44*(13), 6868–6875. https://doi.org/10.1002/2017GL073656

Wang, Z., Turner, J., Wu, Y., & Liu, C. (2019). Rapid Decline of Total Antarctic Sea Ice Extent during 2014–16 Controlled by Wind-Driven Sea Ice Drift. *Journal of Climate*, *32*(17), 5381–5395. https://doi.org/10.1175/JCLI-D-18-0635.1

Zhang, J., & Rothrock, D. A. (2003). Modeling Global Sea Ice with a Thickness and Enthalpy Distribution Model in Generalized Curvilinear Coordinates. *MONTHLY WEATHER REVIEW*, *131*, 17.